Journal of Engg. Research **Vol. 5 No. (3) September 2017 pp.** *198-215*

تحليل عددي للمعامل الكهرومغناطيسية الناتجة عن الحمل الثنائي الممغنط المهيمَن حراريا

شمس الدين المعاتقي[،***]، لواء القلسي[**،***]، كوثر غشام[**]، عبد العزيز سالم الغامدي[*]، محمد ناصر البرجيني[**] والحبيب بن عيسية[**]**

[*] كلية الهندسة، قسم الهندسة الميكانيكية، جامعة حائل، المملكة العربية السعودية

[**] وحدة البحث في علم القياس و أنظمة الطاقة، المدرسة الوطنية للمهندسين بالمنستير، جامعة المنستير، الجمهورية التونسية

[***] المدرسة الوطنية للمهندسين ببنزرت، جامعة قرطاج، الجمهورية التونسية

الخـلاصـة

تتمثل هذه الدراسة في تحليل عددي للمعامل الكهرومغناطيسية، للهيدروديناميكا المغناطيسية للحمل الحراري الطبيعي الثنائي بوجود حقل مغناطيسي خارجي منتظم في تجويف مكعب. وتم تثبيت الحدين العموديين في درجتي حرارة وتركيزين مختلفين مع وجود حقل مغناطيسي منتظم في الاتجاه X. حلت المعادلات ثلاثية الأبعاد باستخدام طريقة الأحجام المحدودة. النتائج المقدمة تتمثل في في كثافة التيار، الجهد الكهربائي، مجال السرعة وطبقة هارتمان، و قد تم الحصول عليها في رقم رايلاي = 10^5 ، رقم لويس = 10، رقم براندت = 10 ونسبة طفو = 0.5- وأرقام هارتمان مختلفة. وتبين من خلال النتائج أن تدرجات الجهد الكهربائي تتغير عكسيا مع تغير شدة المجال المغناطيسي. بالنسبة لأرقام هارتمان المنخفضة، يكون مجال سيران التيار الكهربائي أكثر ارتصاصا بالقرب من الجدران النشطة. زيادة حجم المجال المغناطيسي يؤدي للحد من كثافة التيار المباشر والتيار المولد الغير المباشر.

Numerical analysis of electromagnetic parameters of thermal dominated double diffusive magneto-convection

C. Maatki**'***, L. Kolsi*'**, K. Ghachem**, A.S. Alghamdi*, M.N. Borjini** and H. Ben Aissïa**

** College of Engineering, Mechanical Engineering Department, Haïl University, Haïl City, Saudi Arabia*

*** Unité de recherche de Métrologie et des Systèmes Energétiques, Ecole Nationale d'Ingénieurs, 5000 Monastir, University of Monastir, Tunisia*

**** Ecole Nationale d'Ingénieurs de Bizerte 7030, University of Carthage, Tunisia*

** Corresponding Author: (lioua_enim@yahoo.fr)*

ABSTRACT

This paper presents a numerical investigation of the electromagnetic parameters of magnetohydrodynamic (MHD) thermosolutal natural convection in a cubic cavity. Verticals sides were maintained at constant temperatures and concentrations, although the other sides are adiabatic. A uniform magnetic field is imposed in the x-direction. Three-dimensional equations of mass conservation, momentum, energy, species, Ohms law and conservation of electric charge were solved using finite volume method. Results in term of current density, electrical potential, velocity field and Hartmann layer, were obtained for Ra = 105, Pr = 10, Le = 10, N = -0.5 and different Hartmann numbers. Many results were deduced from this work. Firstly, the electrical potential gradients are inversely proportional to the magnetic field intensity. In addition, for low Hartmann numbers, the current circulation is more pronounced near of the active walls. In addition, the increase of magnitude of magnetic field causes the reduction of the density of the direct and indirect induced current.

NOMENCLATURE

$\vec{B}$: magnetic field ($=\vec{B}'/B_0$).
C: dimensionless concentration $(C'-C'_l)/(C'_h-C'_l)$.
C'$_h$: High species concentration.
C'$_l$: Low species concentration.
D: Species diffusivity.
$\vec{e}_x$: Direction of magnetic field.
g: Acceleration of gravity.
Ha: Hartmann number.
$\vec{J}$: Dimensionless current density ($=\vec{J}'/(\sigma.v_0.B_0^2)$).
L: Cavity side.
Le: Lewis number.
N: Buoyancy ratio.
$\overline{Nu}$: Average Nusselt number.
$\vec{n}$: Normal unit vector.
R: Correlation coefficient.
$\overline{Sh}$: Average Sherwood number.
T: Dimensionless temperature $(=(T'-T_c)/(T'_h-T_c))$
t: Dimensionless time ($=t'.\alpha/L^2$).
T'$_h$: Hot wall temperature.
T'$_c$: Cold wall temperature.
$\vec{u}$: Dimensionless velocity ($=\vec{u}'.L/\alpha$).

Greek symbols

α: Thermal diffusivity.
β_T: Coefficient of thermal expansion.
β_C: Coefficient of compositional expansion.
$\delta_\perp$: Hartmann boundary layer.
Φ: Dimensionless electric potential.
μ: Dynamic viscosity.
ν: Kinematic viscosity.
σ_e: Electrical conductivity.
$\vec{\omega}$: Dimensionless vorticity ($=\vec{\omega}'.\alpha/l^2$).
$\vec{\psi}$: Dimensionless stream function ($\vec{\psi}'/\alpha$).

Superscripts

`: Dimensional variable.

Subscripts

x, y, z: Cartesian coordinates.

INTRODUCTION

Double diffusive natural convection is one of the fundamental problems of the convective heat transfer. It is important in many engineering applications, such as the foundries and the process of solidification (e.g., in crystal growth process). Because of the electric conductivity of some binary mixtures, the flow can be influenced by an external magnetic field; indeed, a MHD flow can be conceived to optimize production processes.

The magnetohydrodynamic natural convection phenomenon with Prandtl number effect inside a square enclosure, having an adiabatic square body, was numerically investigated by Hussein *et al*. (2016). They found that, for high Hartmann number, the magnetic field has a strong influence on the flow field especially when the Prandtl number is high. They also showed that, for Hartmann numbers up to 10, the flow field is slightly affected by MHD effects. On the opposite side, when the Hartmann numbers jump to 50, MHD forces dominate while inertial forces become insignificant.

A numerical analysis, to predict the effect of electrical wall conductivity and magnetic field direction on natural convective flow in a cavity, was studied by Mohamed *et al*. (2016). They showed that the vertically directed magnetic field is the most effective in controlling the flow. The authors found that the wall electrical conductivity enhances damping by changing the distribution of the induced electric current, which augments the magnitude of the Lorentz force.

The influence of the magnetic field on the entropy generation and heat and mass transfer is studied by Maatki *et al*. (2016a). The main important result in their study is that the increase of Hartmann number damped the flow and homogenized the entropy generation distribution in the entire cavity.

In recent years, high magnetic fields have been applied in protein crystallization. Da-Chuan Yin (2015) found that a magnetic field could align the crystals along the field direction. In addition, he showed that a suitable inhomogeneous magnetic field could damp the natural convection. He showed that a high magnitude of magnetic fields improve the quality of some protein crystals.

These discoveries showed that the researches on protein crystallization in high magnetic field are potentially valuable, because obtaining high-quality protein crystals is important for 3D structure.

A few papers have considered the 3D double diffusive natural convection. Bergeon & Knobloch (2002) studied bifurcations in the double diffusive convection in a 3D cavity subjected to horizontal concentration and temperature gradients. They found that the flow is unstable and periodic. The oscillations were found to be an indirect consequence of the presence of a bifurcation in the longitudinal structures of the three-dimensional flow, which cannot be detected in a two-dimensional configuration. Sezai & Mohamad (2000) demonstrated that, in the case of a cubic cavity, the flow structure, for values of buoyancy number greater than unity, is purely three-dimensional. They noticed a variety of bifurcations and the formation of complex flow configurations. Abidi *et al*. (2008) studied the same configuration with heat and mass diffusive horizontal walls. They found that the effect of the heat and mass diffusive walls is the reduction of the transverse velocity for the thermal buoyancy-dominated regime and the increase in it considerably for the compositional buoyancy-dominated regime. Kuznetsov *et al*. (2011) numerically analyzed the effect of the Rayleigh number and the conductivity ratio on heat and mass transfer in the case of transient thermosolutal convection in an air-filled cubic enclosure, with finite thickness walls being exposed to temperature and concentration gradients.

The magnetohydrodynamic double diffusive natural convection in 3D configuration is less investigated. Abd El-Aziz (2008) studied the effects of blowing/suction, thermal-diffusion, and diffusion-thermo on hydromagnetic three-dimensional free convective heat and mass transfer from an inclined stretching surface in the presence of radiation. The author mentioned that the increase of the magnetic field magnitude leads to a significant decrease in the velocity and an increase in the temperature and concentration of the fluid, and the maximum effect of the thermal-diffusion and diffusion-thermo on the velocity occurs in the absence of the magnetic field when the plate is impermeable. Maatki *et al*. (2013) investigated the three-dimensional effects of thermosolutal natural convection in a cubic enclosure subject to horizontal and opposing gradients of heat and solutal transfers in the presence of magnetic field. Different patterns of flow were observed with changing in the intensity of the magnetic field and the different forcing situations. They also mentioned that increasing the intensity of the magnetic field causes a monotonic reduction of the intensity of the main flow, the intensity of the transverse flow, and the intensity of heat and mass transfer.

Recently, Maatki *et al*. (2016b) studied the effect of the magnetic field inclination on 3D double diffusive convection in a cubic cavity filled with a binary mixture. They showed that the increase of the inclination of the magnetic field direction damped the flow. In addition, they found a critical angle, which, depending on the Hartmann number, caused a big change in the flow structure and accented the three-dimensional aspect in the cavity.

It is in this context that the present work investigates the effect of the magnetic field magnitude on the electromagnetic parameters in the case of a 3D thermally dominated double diffusive natural convection in a cube-shaped cavity filled with a binary mixture (protein solution).

MATHEMATICAL FORMULATION

The geometry under consideration (Figure 1) is a cubic cavity, filled with a binary mixture (protein solution), and characterized by *Pr* and *Le* numbers both equal to 10. Different temperatures and concentrations are specified between the left (T'_c, C'_l) and right vertical walls (T'_h, C'_h). Zero heat and mass fluxes are imposed on the remaining walls with non-slip boundary conditions, and a homogeneous magnetic field expressed by $B_0.\vec{e}_B$ is imposed perpendicular to the heated walls.

Under the effect of the magnetic field, additional dimensionless numbers appear. In fact, in addition to the Rayleigh and Prandtl numbers, the flow becomes controlled also by the magnetic Reynolds number, defined as $R_m = \mu.\sigma.\upsilon_0.L$, and the Hartmann number, given by $Ha = \sqrt{\frac{B_0^2.L^2.\sigma_e}{\rho.\nu}}$.

In these expressions, μ is the magnetic permeability, ρ is the density, σ_e is the electric conductivity, $\upsilon_0 = \frac{\alpha}{L}$ is the characteristic velocity, ν is the kinematic viscosity, and α is the thermal diffusivity.

The magnetic Reynolds number represents the ratio between the induced magnetic field by the movement of the fluid and the applied magnetic field. The Hartmann number represents the ratio between the Lorentz forces, produced by the interaction of the current density $\vec{j}'$ with the applied magnetic field $\vec{B}'$, and the viscosity forces.

The flow is assumed to be laminar and incompressible, and the binary fluid is assumed to be Newtonian. The physical properties of the fluid are supposed to be constant, and the Boussinesq approximation is adopted. The Soret and Dufour effects are assumed to be negligible, and the magnetic Reynolds number is assumed to be so small so that the induced magnetic field is insignificant.

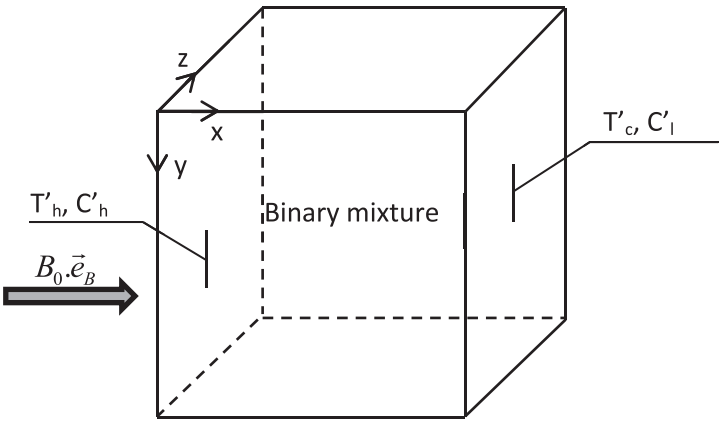

Figure 1. Geometric configuration with coordinates.

The movement of the fluid is induced by the variations of the density caused by the gradients of temperature. The presence of the magnetic field will cause the Lorentz force, given by the following:

$$\vec{F}' = \rho_e.\vec{E}' + \vec{J}' \times \vec{B}' \tag{1}$$

with $\vec{E}' = -\vec{\nabla}\Phi'$

where ρ_e is the density of electric charge, $.\vec{E}$ is the electric field, and Φ' is the electric potential.

In addition, for a moving medium, the density of the electrical current is governed by the generalized Ohm's law, which is written as follows:

$$\vec{J}' = \rho_e.\vec{V}' + \sigma\left(-\vec{\nabla}\Phi' + \vec{V}' \times \vec{B}'\right) \tag{2}$$

with $\vec{V}'$ being the velocity vector.

ρ_e is usually very small, so the terms $\rho_e..\vec{E}$ and $\rho_e.\vec{V}'$ in the Equations (1) and (2) are negligible. $\vec{B}'$ is composed of the applied magnetic field $B_0.\vec{e}_B$ and the induced magnetic field produced by the electrical currents. Indeed, R_m is weak and we can neglect the induced magnetic field, and the Hartmann number becomes the only additional parameter related to the external applied magnetic field. A discussion on the limits of validity of the low magnetic Reynolds number approximation can be found in the work of Sarris *et al*. (2006).

In addition to the Ohm's law, the density of electrical current $\vec{J}'$ is governed by the conservation law:

$$\vec{\nabla}.\vec{J}' = 0 \tag{3}$$

Thus, by adding the relations relating to the presence of the external magnetic field to those of an ordinary hydrodynamic flow and using the dimensionless variables, the equations describing the problem of the magnetohydrodynamic double diffusive natural convection are the equations of continuity, momentum, energy, species, Ohm's law, and conservation of electric charge.

The dimensionless variables used in this work are as follows:

$$(x,y,z) = \frac{(x',y',z')}{L},\ B = B'/B_0,\ \Phi = \Phi'/\left(l.\upsilon_0.B_0\right),\ J = J'/\left(\sigma.\upsilon_0.B_0\right),\ C = \frac{C'-C'_l}{C_h - C_l},\ T = \frac{T'-T'_C}{T_h - T_C},$$

$$(u_x,u_y,u_z) = \frac{(u'_x,u'_y,u'_z)L}{\alpha} \text{ and } t = \frac{t'}{\alpha L^2}$$

For the numerical method, potential-vorticity vector formalism in vector form in a three-dimensional configuration is used (Kolsi *et al*. (2007)). The vorticity and potential vectors are defined by the following relations, respectively: $\vec{\omega} = \vec{\nabla} \times \vec{u}$ (1), $\vec{u} = \vec{\nabla} \times \vec{\psi}$ (4)

The dimensional equations of conservation describing the phenomenon are written in the following form:

$$\vec{\nabla}^2\vec{\psi} = -\vec{\omega} \tag{5}$$

$$\frac{\partial \vec{\omega}}{\partial t} + (\vec{u}\vec{\nabla})\vec{\omega} - (\vec{\omega}\vec{\nabla})\vec{u} = \Pr \vec{\nabla}^2 \vec{\omega} + Ra \Pr\left[\frac{\partial T}{\partial z}, 0, -\frac{\partial T}{\partial x}\right] - Ra \Pr N\left[\frac{\partial C}{\partial z}, 0, -\frac{\partial C}{\partial x}\right] \quad (6)$$
$$+ \Pr Ha^2 (\vec{\nabla} \times (\vec{j} \times \vec{e}_x))$$

$$\frac{\partial T}{\partial t} + \vec{u}\vec{\nabla} T = \vec{\nabla}^2 T \quad (7)$$

$$\frac{\partial C}{\partial t} + \vec{u}\vec{\nabla} C = \frac{1}{Le}\vec{\nabla}^2 C \quad (8)$$

$$\vec{j} = -\vec{\nabla}\Phi + \vec{u} \times \vec{e}_x \quad (9)$$

$$\vec{\nabla}^2 \Phi = \vec{\nabla}(\vec{u} \times \vec{B}) = -\vec{e}_x \vec{\omega} \quad (10)$$

The dimensionless parameters in the above equations are defined as follows:

$$N = \frac{\beta_c (C_h - C_l)}{\beta_T (T_h - T_C)}, Ha = B_0 L \sqrt{\frac{\sigma_e}{\rho \nu}}, Ra = \frac{g\beta_T (T_h - T_C) L^3}{\nu.\alpha}, \Pr = \frac{\nu}{\alpha} \text{ and } Le = \frac{\alpha}{D}$$

and they represent, respectively, the buoyancy ratio and the Hartmann, Rayleigh, Prandtl, and Lewis numbers.

The temperature and concentration boundary conditions are given by

$T(0, y, z) = 1$; $C(0, y, z) = 1$; $\frac{\partial T}{\partial n} = 0$ and $\frac{\partial C}{\partial n} = 0$ on other walls.
$T(1, y, z) = 0$ $C(1, y, z) = 0$

The boundary conditions regarding vorticity and potential vector of velocity (Kolsi *et al.* (2007)) are as follows:

- Vorticity

$$\omega_x = 0,\ \omega_y = -\frac{\partial u_z}{\partial x},\ \omega_z = \frac{\partial u_y}{\partial x} \text{ at } x = 0 \text{ and } 1$$

$$\omega_x = \frac{\partial u_z}{\partial y},\ \omega_y = 0,\ \omega_z = -\frac{\partial u_x}{\partial y} \text{ at } y = 0 \text{ and } 1$$

$$\omega_x = -\frac{\partial u_y}{\partial z},\ \omega_y = \frac{\partial u_x}{\partial z},\ \omega_z = 0 \text{ at } z = 0 \text{ and } 1$$

- Vector potential

$$\frac{\partial \psi_x}{\partial x} = \psi_y = \psi_z = 0 \text{ at } x = 0 \text{ and } 1$$

$$\psi_x = \frac{\partial \psi_y}{\partial y} = \psi_z = 0 \text{ at } y = 0 \text{ and } 1$$

$$\psi_x = \psi_y = \frac{\partial \psi_z}{\partial z} = 0 \text{ at } z = 0 \text{ and } 1$$

The boundary conditions related to velocity, electric potential, and current density on the inner surface are as follows:

- Velocity: $u_x = u_y = u_z = 0$ on all walls
- Electric potential : $\frac{\partial \Phi}{\partial n} = 0$ on all walls
- Current density: $\vec{J}.\vec{n} = 0$ on all walls

NUMERICAL APPROACH GRID DEPENDENCY AND VALIDATION

The control volume finite difference method is used to discretize Equations (5)-(10). The power law scheme for treating convective-diffusion terms and the fully implicit procedure to discretize the temporal derivatives are retained. The grid is uniform in all directions with additional nodes on the boundaries. The successive relaxation iterating scheme is used to solve the resulting non-linear algebraic equations. The system is coded in FORTRAN language.

The general equation is as given by Patankar (1980) as follows:

$$\frac{\partial \Phi}{\partial t} + \frac{\partial L_x}{\partial x} + \frac{\partial L_y}{\partial y} + \frac{\partial L_z}{\partial z} = S_\Phi \tag{11}$$

where

L_x, L_y, L_z represent the total flow of convection and diffusion in the directions x, y, and z, respectively.

$$L_x = V_x.\Phi - \Gamma_\Phi \frac{\partial \Phi}{\partial x}, L_y = V_y.\Phi - \Gamma_\Phi \frac{\partial \Phi}{\partial y} \text{ and } L_z = V_z.\Phi - \Gamma_\Phi \frac{\partial \Phi}{\partial z} \tag{12}$$

where Φ can be T, C, ω_x, ω_y or ω_z

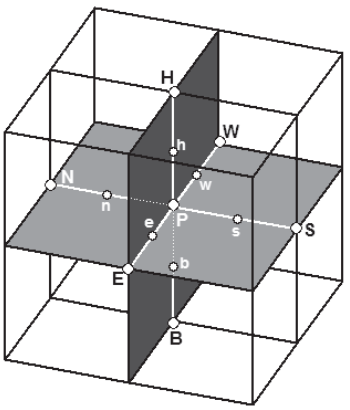

Figure 2. 3D control volume.

The integration of the general Equation (11) on a control volume gives the following:

$$\left(\Phi_p - \Phi_p^\circ\right).\Delta x.\Delta y.\Delta z + \left(L_{xe} - L_{xw}\right).\Delta y.\Delta z.\Delta t + \left(L_{yn} - L_{ys}\right).\Delta x.\Delta z.\Delta t + \left(L_{zh} - L_{zb}\right).\Delta x.\Delta y.\Delta t = \overline{S}.\Delta x.\Delta y.\Delta z.\Delta t \tag{13}$$

where e, w, s, f, b, and p represent the east, west, north, south, front, back, and central nodes of the control volume; and ° is used to indicate the variable to be calculated at a preceding instant (Figure 2).

Using the parameters

$$L_e = L_{xe}.\Delta y.\Delta z \text{ et } L_w = L_{xw}.\Delta y.\Delta z;$$

$$L_n = L_{yn}.\Delta x.\Delta z \text{ et } L_s = L_{ys}.\Delta x.\Delta z; \tag{14}$$

$$L_h = L_{zh}.\Delta x.\Delta y \text{ et } L_b = L_{zb}.\Delta x.\Delta y$$

the equation becomes

$$\left(\Phi_p - \Phi_p^{\circ}\right)\frac{\Delta x.\Delta y.\Delta z}{\Delta t} + \left(L_e - L_w\right) + \left(L_n - L_s\right) + \left(L_h - L_b\right) = \overline{S}\,\Delta x\Delta y.\Delta z \tag{15}$$

The source term is linear and it is written as follows:

$$\overline{S} = S_c + S_p\Phi_p \tag{16}$$

By referring to the work of Patankar (1980), the system of equations becomes as follows:

$$\left(L_n - F_n\Phi_p\right) = a_N\left(\Phi_p - \Phi_N\right)$$
$$\left(L_s - F_s\Phi_p\right) = a_S\left(\Phi_S - \Phi_p\right)$$
$$\left(L_e - F_e\Phi_p\right) = a_E\left(\Phi_p - \Phi_E\right)$$
$$\left(L_w - F_w\Phi_p\right) = a_W\left(\Phi_W - \Phi_p\right)$$
$$\left(L_h - F_h\Phi_p\right) = a_H\left(\Phi_p - \Phi_H\right)$$
$$\left(L_b - F_b\Phi_p\right) = a_B\left(\Phi_B - \Phi_p\right)$$

$$\rightarrow a_p\Phi_p = a_E\Phi_E + a_W\Phi_W + a_N\Phi_N + a_S\Phi_S + a_H\Phi_H + a_B\Phi_B + b_p \tag{17}$$

The coefficients of Equation (17) are as follows:

$$a_p = a_E + a_W + a_N + a_S + a_H + a_B + \frac{\Delta x.\Delta y.\Delta z}{\Delta t} - S_p.\Delta x.\Delta y.\Delta z$$

$$b_p = S_c.\Delta x.\Delta y.\Delta z + \Phi_p^{\circ}\frac{\Delta x.\Delta y.\Delta z}{\Delta t}$$

The solution is considered acceptable when the following convergence criterion is satisfied for each step of time:

$$\sum_{i}^{1,2,3}\frac{\max\left|\psi_i^n - \psi_i^{n-1}\right|}{\max\left|\psi_i^n\right|} + \max\left|T_i^n - T_i^{n-1}\right| + \max\left|C_i^n - C_i^{n-1}\right| \le 10^{-5} \tag{18}$$

More information on the numerical method can be found in the work of Kolsi *et al*. (2007). Table 1 shows that a grid of size 51x51x51 is satisfying for this study. The code is validated against the results of magnetohydrodynamic buoyancy induced convection in enclosures presented by Chamkha *et al*. (2002) (Table 2) and the results of three-dimensional double diffusive convection in a cubic enclosure obtained by Sezai & Mohamed (2000) (Figure 3). A quasi-perfect concordance is noticed.

Table 1. Grid dependency for Ra = 105, Pr = 10, Le = 10, and N = -0.5.

Grid	31x31x31	41x41x41	51x51x51	61x61x61
$\overline{Nu}$	3.734	3.895	4.023	4.030
$\overline{Sh}$	7.174	7.268	7.328	7.331

Table 2. Comparison between the present results and literature for Ra=105, Pr =1, Le =2, and N=1.

Ha	Authors	$\overline{Nu}$	$\overline{Sh}$
0	Present result (Chamkha *et al*. (2000))	3,358 (3,319)	4,078 (4,030)
5	Present result (Chamkha *et al*. (2000))	3,247 (3,215)	3,948 (3,909)
10	Present result (Chamkha *et al*. (2000))	3,093 (3,048)	3,853 (3,797)
15	Present result (Chamkha *et al*. (2000))	2,905 (2,868)	3,792 (3,744)
20	Present result (Chamkha *et al*. (2000))	2,539 (2,497)	3,714 (3,652)

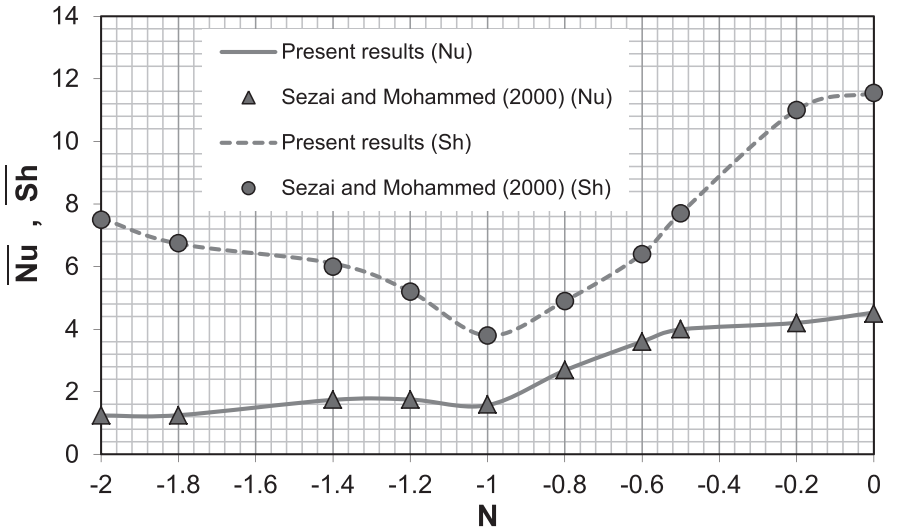

Fig. 3. Comparison between the present results and those of Sezai & Mohamed (2000) (Ra=105, Pr=10, and Le=10).

RESULTS AND DISCUSSION

In this work, the effect of the magnetic field is on the 3D thermosolutal convection, with a special focus on the electromagnetic parameters. The Rayleigh number, Prandtl number, Lewis number, and buoyancy ratio are, respectively, fixed at $Ra=10^5$, Pr=10, Le=10, and N=-0.5.

Figure 4 illustrates the 3D distribution of the Lorentz force for different Hartmann numbers. The increase in the Hartmann number causes an increase in the Lorentz force. This force has a Gaussian form and is more importantly near the cold wall, inducing a reduction of the buoyancy forces.

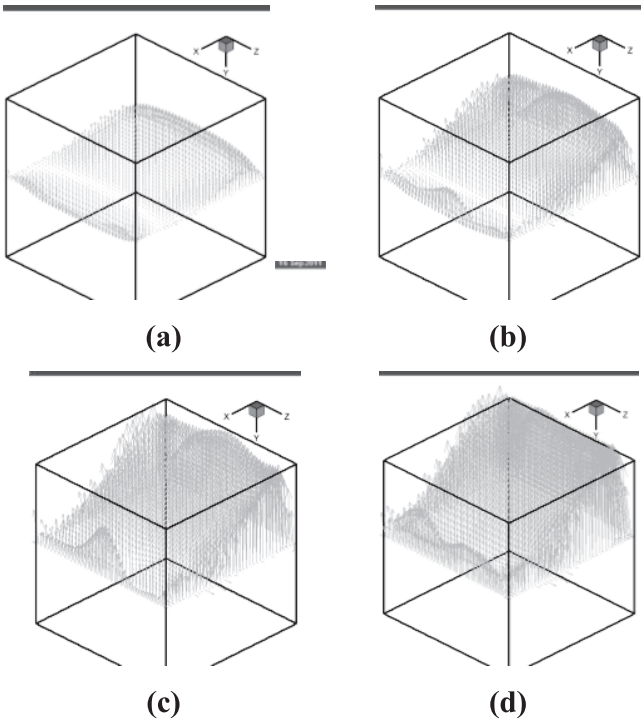

Figure 4. Lorentz force vectors at y=0.5 plan for different Hartman numbers; (a) Ha=20, (b) Ha=40, (c) Ha=50, (d) Ha=60.

Figure 5(a) presents the 3D distribution of velocity vectors at y=0.5 plan in the case of thermal dominated convection and without magnetic field. The velocity vectors near the active walls are greater than those located at the central region of the cavity. It is noticed that there is a predominance of the y-component of the velocity due to the floatability force.

The interaction between the magnetic field and the fluid motion creates an induced current. This current is the cause of producing the Lorentz force, which opposes the floatability force and reduces the intensity of the flow. Figure 5(d) shows the deceleration of the flow caused by applying the magnetic field.

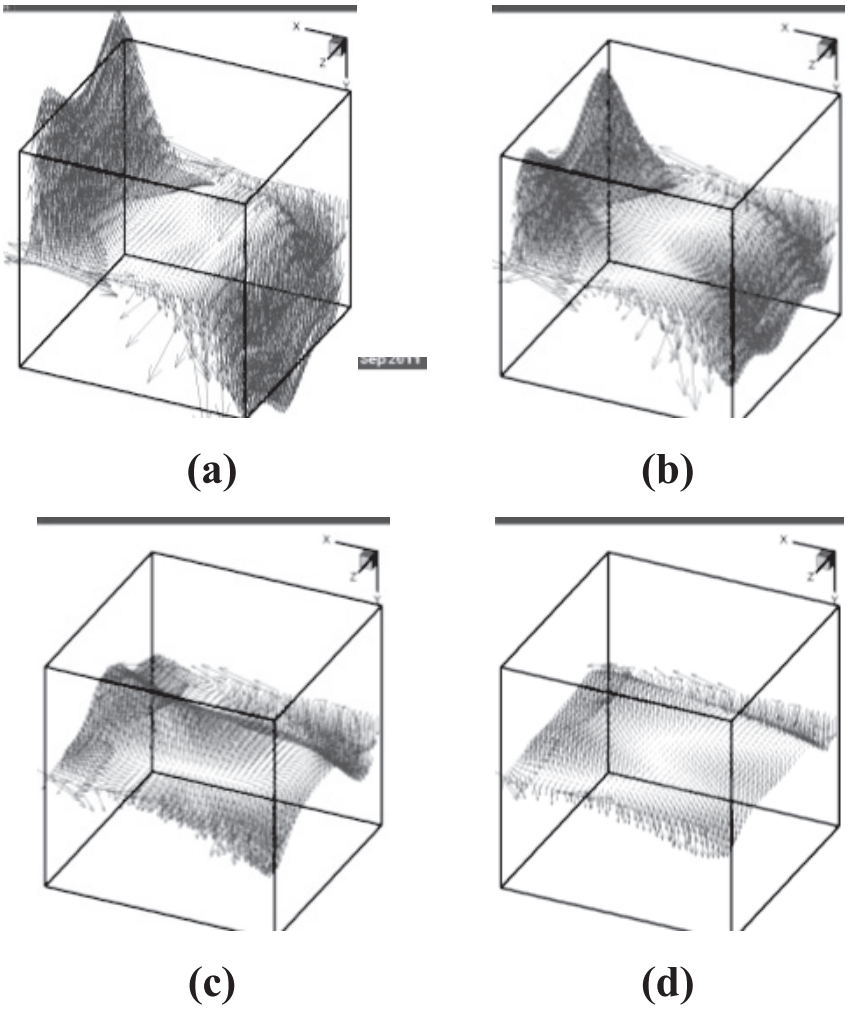

Figure 5. Velocity vectors at y=0.5 plan for different Hartman numbers;
(a) Ha=0, (b) Ha=20, (c) Ha=40, (d) Ha=60.

Figure 6 presents the effect of the magnetic field on the distribution of the direct induced current at y=0.5 plan. For Ha=10 (Figure 6(a)), the current circulation is more pronounced near the active walls. The direct induced current is given by ($\vec{J}_1 = \vec{V} \times \vec{e}_B$). The velocity vectors near the active walls are principally in the y-direction, and the imposed magnetic field is in the x-direction; that is why the direct induced current is important in those regions.

As seen in Figures 6(b), 6(c), and 6(d), an increase in the magnetic field magnitude causes a reduction in the density of the direct induced current; this reduction is due to the decrease in the velocity.

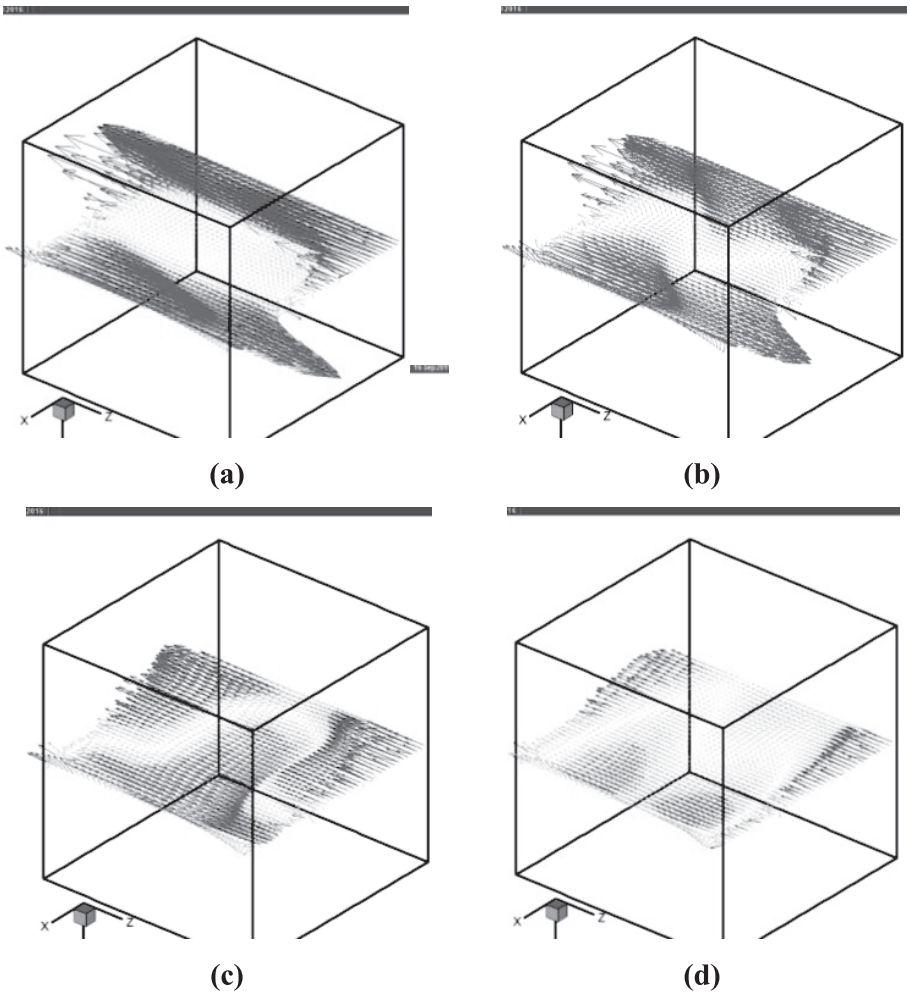

Figure 6. Direct induced current density ($\vec{j}_1$) at y=0.5 plan for different Hartman numbers;

(a) Ha=0, (b) Ha=20, (c) Ha=40, (d) Ha=60.

Figure 6 shows that, for all Hartmann numbers, there is no recirculation of the direct induced current ($\vec{j}_1$) (i.e., (div $\vec{j}_1 \neq 0$)), and there is an accumulation of electrical charge in some regions. This accumulation creates electrical potentials. The current is principally in the z-direction. Consequently, the created electrical potentials are in the form of surfaces perpendicular to the z-direction as seen in Figure 7. The iso-contours of electrical potentials in the plan x=0.5 are distorted. The increase in the magnitude of the magnetic field reduced this distortion. At the vicinity of the corners, there is a concentration of the iso-surfaces of the electrical potentials with a three-dimensional distribution. This concentration creates an indirect induced current density allowing the recirculation of the total current density near the electrically insulated walls.

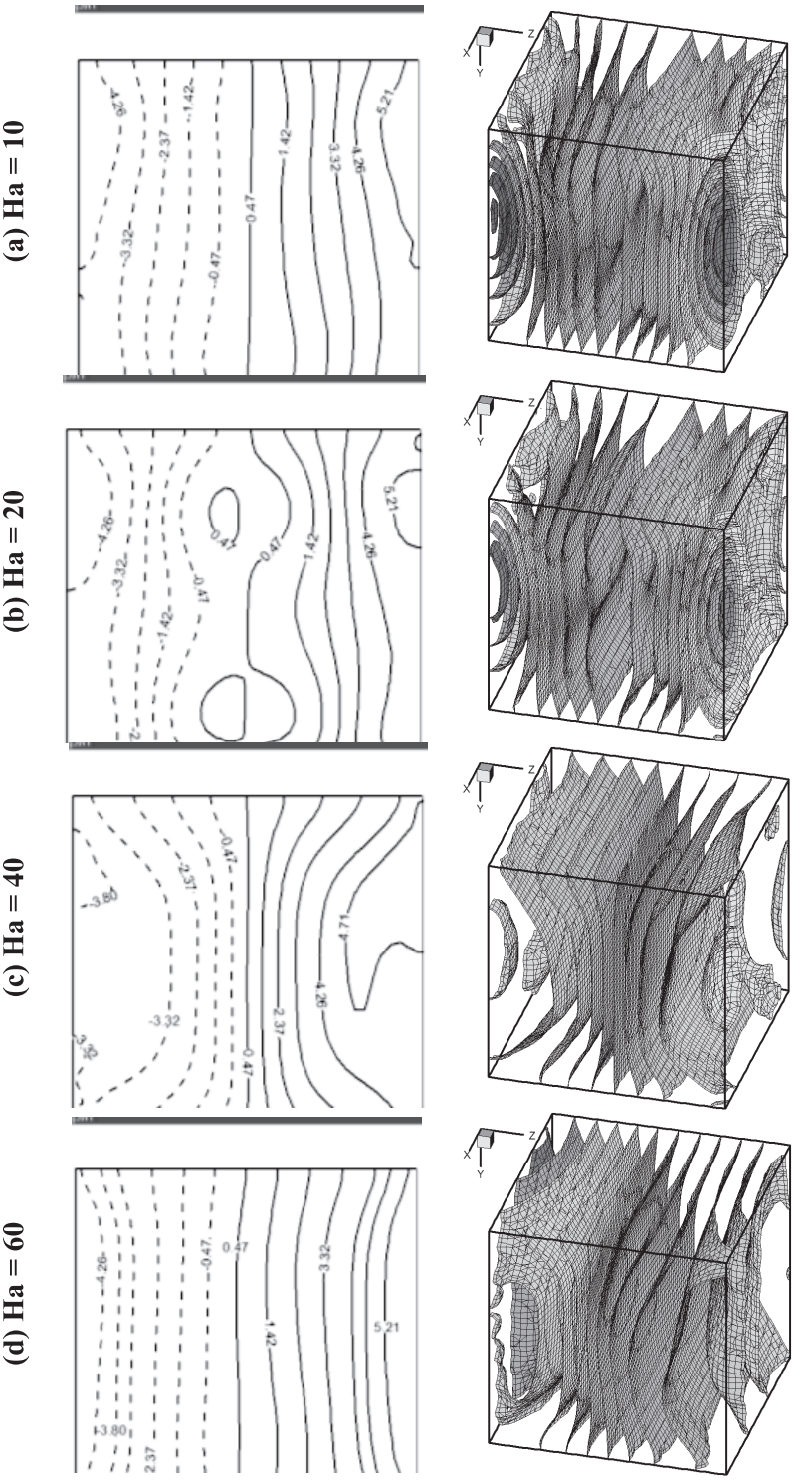

Figure 7. Iso-contours at x=0.5 (left) and iso-surfaces (right) of electrical potential for different Hartmann numbers.

Figure 8 presents the distribution of the indirect induced current ($\vec{j}_2$), in y=0.5 plan for different Hartmann numbers. This current is induced by the electrical potential. It is noticed from Figures 7(a) and 7(b) that the indirect induced current is more intense near the corners. This is due to great gradients of the electrical potentials in those regions. Figures 8(c) and 8(d) show that the intensity of the indirect induced current is reduced by increasing the Hartman number in all regions of the cavity. This reduction is the result of the decrease in electrical potential gradients by increasing the magnitude of the magnetic field.

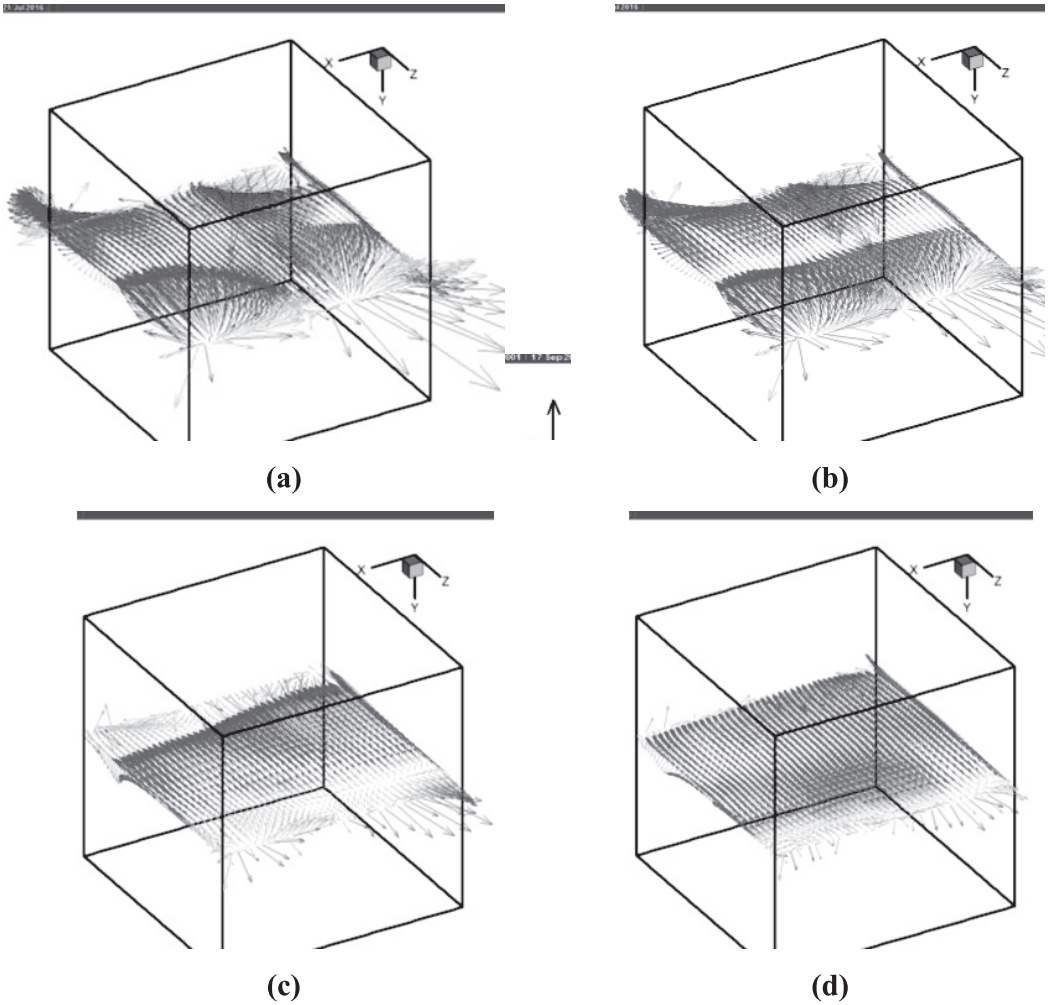

Figure 8. Indirect induced current density ($\vec{j}_2$) at y=0.5 plan for different Hartman numbers; (a) Ha=0, (b) Ha=20, (c) Ha=40, (d): Ha=60.

The density of the total induced current is presented in Figure 9. This figure shows the existence of a recirculation of the current near the insulated adiabatic walls. This effect is caused by the indirect current ($\vec{j}_2$). The increase in the Hartman number causes an attenuation of the total current and disappearance of recirculation zones.

Due to the interaction of the induced electric current with the applied magnetic field, two boundary layers develop in the vicinity of the active walls. These layers, called Hartmann boundary layers, represent one of the most important characteristic features of the MHD flows. Gradients of velocity and current density are concentrated in these layers.

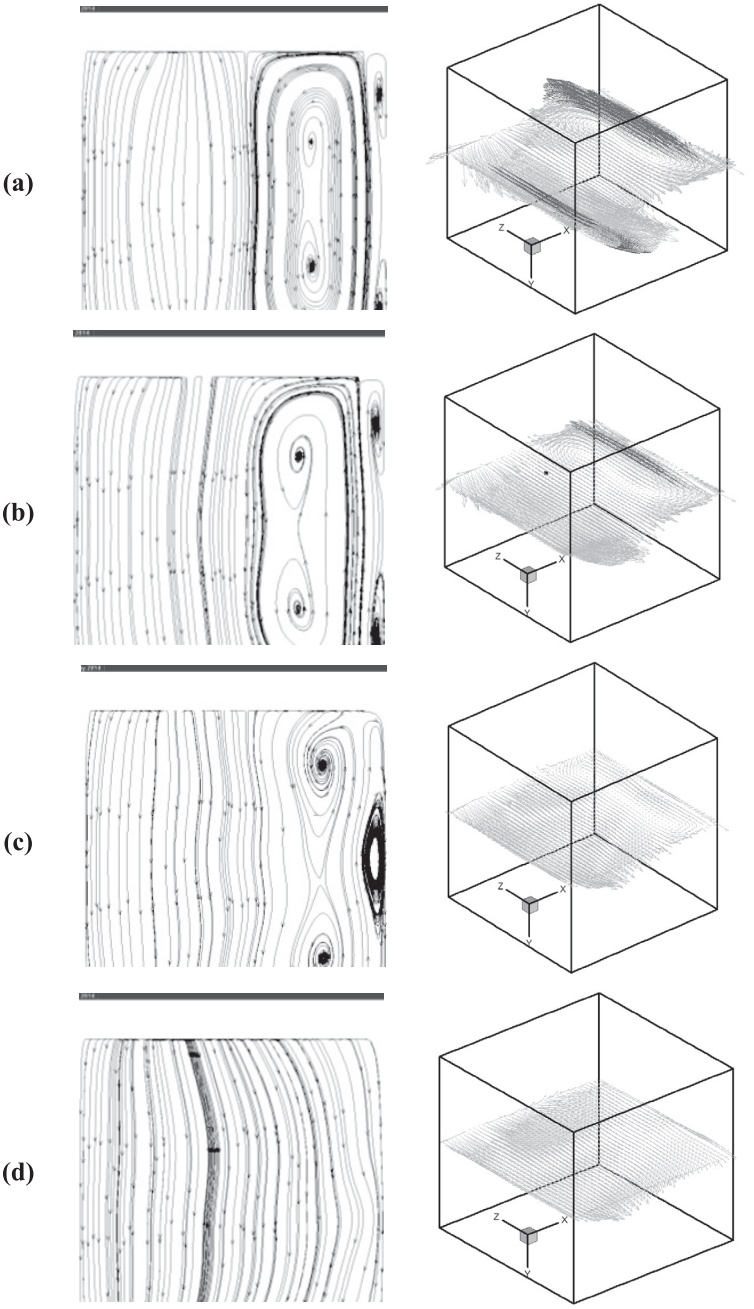

Figure 9. Total induced current density ($\vec{j}$) at y=0.5 plan for different Hartman numbers; (a) Ha=0, (b) Ha=20, (c) Ha=40, (d): Ha=60.

The variation of the Hartmann boundary layer thickness is presented in Figure 10, and as predicted, this thickness decreases with the Hartmann number. Tow correlations corresponding to tow ranges of Hartmann numbers are determined as follows:

For : $Ha \leq 50 \; : \; \delta_{\perp} = 0{,}5345.\dfrac{1}{Ha^{0{,}659}} \; with \; R^2=0{,}9699$

For : $Ha > 50 : \delta_{\perp} = 1{,}275.\dfrac{1}{Ha^{0{,}9}} \; with \; R^2=0{,}9749$

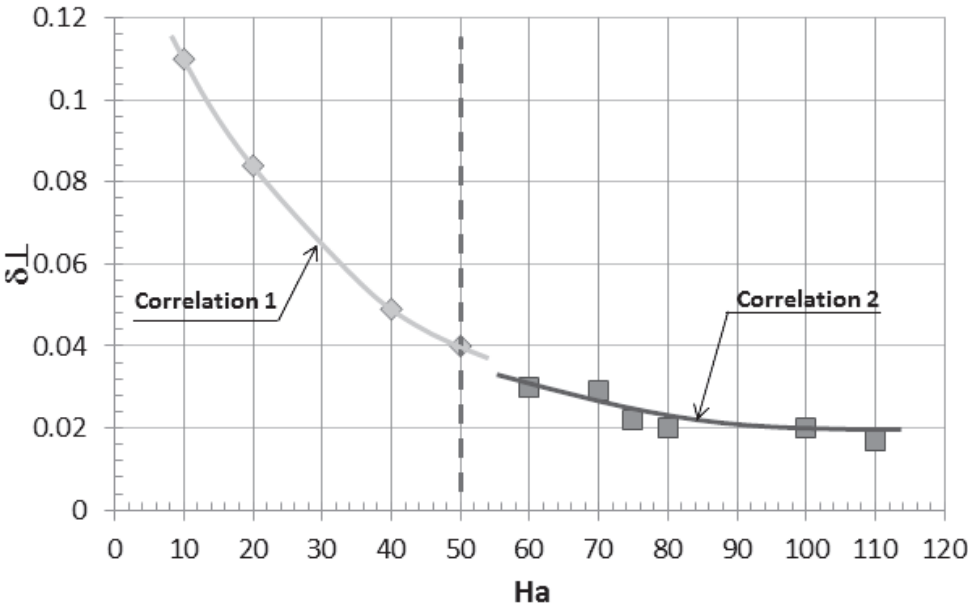

Figure 10. Hartmann boundary layer thickness versus Hartmann number.

CONCLUSIONS

A numerical study was performed to examine the effect of magnetic field on electromagnetic parameters of a 3D double diffusive natural convection in a cubic cavity filled with a binary mixture. The governing equations in a 3D vector potential-vorticity form were solved with the finite volume method. Graphical results for the electrical potential, current densities, velocity field, and Hartmann boundary layer for different intensities of the magnetic field were presented and discussed. The obtained results showed the following:

- ✓ The reduction of the velocity by increasing the Hartmann number.
- ✓ For all Hartmann numbers, the velocity augments from zero near the walls to a maximal value situated in the viscous boundary layer.
- ✓ The produced electrical current is due to the fluid motion.
- ✓ Near the electrically insulated walls, the current lines are closed due to current conservation.
- ✓ The produced Lorentz force opposes and brakes the convective flow.

REFERENCES

Abidi, A. Kolsi, L. Borjini, M. N. Ben Aissia, H. & Safi, M. J. 2008. Effect of heat and mass transfer through diffusive walls on three-dimensional double-diffusive natural convection. Numerical Heat Transfer, Part A, **53**: 1357–1376

Adegun, I.K. 2016. Modeling of MHD natural convection in a square enclosure having an adiabatic square shaped body using Lattice Boltzmann Method. Alexandria Engineering Journal, **55**(1): 203–214.

Abd El-Aziz, M. 2008. Thermal-diffusion and diffusion-thermo effects on combined heat and mass transfer by hydromagnetic three-dimensional free convection over a permeable stretching surface with radiation. Physics Letters A, **372**: 263–272.

Bergeon, A. & Knobloch, E. 2002. Natural doubly diffusive convection in three-dimensional enclosures, Physics of fluids, **14**: 3233-3250.

Chamkha, A.J. & Al-Naser, H. 2002. Hydromagnetic double-diffuse convection in a rectangular enclosure with opposing temperature and concentration gradients. Int. J. Heat Mass Transfer, **45**: 2465– 2483.

Hussein, A.K., H.R. Ashorynejad, S., Sivasankaran, S., Kolsi, L., Shikholeslami, M.,

Kolsi, L., Abidi, A., Borjini, M.N., Daous, N. & Ben Aissia, H. 2007. Effect of an external magnetic field on the 3-D unsteady natural convection in a cubical enclosure. Numerical Heat Transfer, Part A, **51**: 1003–1021.

Kuznetsov, G. V. & Sheremet, M. A. 2011. A numerical simulation of double-diffusive conjugate natural convection in an enclosure. Int. J. Thermal Sci., **50**: 1878-1876.

Maatki, C., Kolsi, L., Oztop, H.F., Chamkha, A., Borjini, M.N., Ben Aissïa, H. & Al-Salem, K. 2013. Effects of magnetic field on 3D double diffusive convection in a cubic cavity filled with a binary mixture. International Communications in Heat and Mass Transfer, **49**: 86–95,

Maatki, C., Hassen, W., Kolsi, L., AlShammari, N., Borjini, M.N. & Aissia, H.B. 2016. 3D numerical study of hydromagnetic double diffusive natural convection and entropy generation in cubic cavity. Journal of Applied Fluid Mechanics, **9**(4): 1915-125.

Maatki, C., Ghachem, K., Kolsi, L., Hussein, A.K., Borjini, M.N. & Ben Aissïa, H. 2016. Inclination effects of magnetic field direction in 3D double-diffusive natural convection. Applied Mathematics and Computation, **273**: 178-189

Mohamed, K. N., Benissaad, S., Berrahil, F. & Talbi, K. 2016. Investigation of magneto hydrodynamic natural convection flows in a 3-D rectangular enclosure. Journal of Applied Fluid Mechanics, **9**(4): 16951708-.

Patankar, S.V. 1980. Numerical heat transfer and fluid flow. McGrawHill, New York.

Sarris, I.E., Zikos, G.K., Grecos, A.P. & Vlachos, N. S. 2006. On the limits of validity of the low magnetic Reynolds number approximation in MHD natural-convection heat transfer. Numerical Heat Transfer, Part B **50**: 157 – 180.

Sezai, I. & Mohamad, A.A. 2000. Double diffusive convection in a cubic enclosure with opposing temperature and concentration gradients. Phys. Fluids, 12: 2210-2223.

Yin, D.C. 2015. Protein crystallization in a magnetic field. Progress in Crystal Growth and Characterization of Materials, **61**(1): 1–26.

Submitted: 10/01/2016
Accepted : 17/01/2017